HHS Public Access

Author manuscript

Nature. Author manuscript; available in PMC 2014 July 16.

Published in final edited form as:

Nature. 2014 January 16; 505(7483): 407–411. doi:10.1038/nature12821.

Perturbed neural activity disrupts cerebral angiogenesis during a postnatal critical period

Christina Whiteus[1,2], **Catarina Freitas**[1], and **Jaime Grutzendler**[1,2,*]

[1]Department of Neurology, Yale University, 300 George St. Suite 8300G, New Haven, CT

[2]Department of Neurobiology, Yale University, 300 George St. Suite 8300G, New Haven, CT 06511

Abstract

During the neonatal period, activity-dependent neural circuit remodeling coincides with growth and refinement of the cerebral microvasculature[1,2]. Whether neural activity also influences the patterning of the vascular bed is not known. Here we show in neonatal mice, that neither reduction of sensory input through whisker trimming nor moderately increased activity by environmental enrichment affected cortical microvascular development. Surprisingly however, chronic stimulation by repetitive sounds, whisker deflection, or motor activity led to a near arrest of angiogenesis in barrel, auditory, and motor cortices, respectively. Chemically-induced seizures also caused robust reductions in microvascular density. Altering neural activity in adult mice, however, did not affect the vasculature. Histological analysis and time-lapse *in vivo* two-photon microscopy revealed that hyperactivity did not lead to cell death or pruning of existing vessels but rather reduced endothelial proliferation and vessel sprouting. This anti-angiogenic effect was prevented by administration of the nitric oxide synthase (NOS) inhibitor L-NAME and in mice with neuronal and inducible NOS deficiency, suggesting that excessive nitric oxide released from hyperactive interneurons and glia inhibited vessel growth. Vascular deficits persisted long after cessation of hyperstimulation, providing evidence for a critical period after which proper microvascular patterning cannot be re-established. Reduced microvascular density diminished the ability of the brain to compensate for hypoxic challenges, leading to dendritic spine loss in regions distant from capillaries. Therefore, excessive sensorimotor stimulation and repetitive neural activation during early childhood may cause lifelong deficits in microvascular reserve, which could have important consequences on brain development, function, and pathology.

*Correspondence and requests for materials should be addressed to jaime.grutzendler@yale.edu, Ph: (203)737-3514, Fax: (203)785-7903.

The authors declare no competing interests.

Author Contributions

Project conception (CW, JG), experimental design (CW, CF, JG), experimental execution (CW, CF), data analysis (CW, CF, JG), manuscript writing (CW, JG).

Supplementary Information is linked to the online version of the paper at www.nature.com/nature.

The development of a cerebral microvascular network that precisely matches regional metabolic demands is crucial given the brain's high energy consumption and susceptibility to ischemia[3]. Though major cerebral vessels form during embryonic development, microvascular sprouting and pruning continue into the neonatal stages[1], concurrent with synaptogenesis, axonal growth, and gliogenesis. Common molecular pathways regulate angiogenesis and axonal growth[4], suggesting that coordinated mechanisms establish a microvascular network that meets the requirements of adjacent neural tissue. While some studies suggest there is a link between neural activity and microvascular plasticity[5–9], this remains controversial and it is unclear whether neural activity regulates vascular development or if angiogenesis follows an autonomous developmental program[10].

To address this question, we examined the effects of neural activity on cerebral microvascular development in neonatal mice. First, we reduced sensory input to the barrel cortex by bilateral whisker trimming for 10 days beginning at p15. This reduces spiking activity and metabolism[11] and affects dendritic spine dynamics[12] in the barrel cortex. We quantified vascular branch points and total length from confocal images of various vascular markers (Supplementary Figure 1a–e, Supplementary Video 1) and found that this manipulation did not affect vascular density in the barrel cortex (Figure 1a, Supplementary Figure 2a,b). Moderate whisker stimulation by environmental enrichment over 10 days also had no effect on microvascular density (Figure 1a, Supplementary Figure 2a,c). Therefore baseline sensory activity does not modulate neonatal cortical angiogenesis.

Surprisingly, more persistent and repetitive activity led to reduced vascular density. Exposure to diverse tones, natural sounds, and white noise over 10 hours daily from p15 to p25 caused robust reductions in vessel branching and length (Figure 1b,c, Supplementary Figure 2a), which increased in magnitude when stimulation was extended (Supplementary Figure 2d). This effect was specific to the stimulated region, as vascular density was reduced in the primary auditory cortex but not in the cingulate cortex (Figure 1b). We then tested the effect of sustained whisker stimulation by performing unilateral whisker trimming and exposing mice to continuous air current. Daily 10-hour stimulation for 8 days led to significant reductions in microvascular density of the barrel cortex corresponding to the stimulated whiskers (Figure 1d, Supplementary Figure 2a). Similarly, 3 hours of daily treadmill running for 5 days reduced vessel density specifically in the motor cortex (Figure 1e, Supplementary Figure 2a). Interestingly, vascular reductions following auditory or whisker stimulations were most apparent in cortical layers 2/3 and 4, while motor hyperactivity had a more significant effect in layers 5 and 6 (Supplementary Figure 2e–g). This is likely due to the fact that sensory cortical layers 2/3 and 4 connect to afferent inputs from the thalamus that are most reliably activated following stimulation[13], while layer 5 efferent neurons in motor cortex are robustly activated during motor output[14].

Over a 10-day period between p15 and 25, repetitive stimulation led to differences of up to 13% in branching and 8% in length between control and stimulated mice. This slight discrepancy is not surprising as most vessels formed postnatally are short capillaries which contribute substantially to branching but less so to length[1]. While this decrease may seem modest, it represents a 70% reduction in the numbers of new vascular branches formed and a 80% reduction in length growth when compared to unmanipulated animals (Figure 1f,g,

Supplementary Figure 2a). In contrast to neonates, chronic auditory stimulation of adult mice did not affect vascular density (Figure 1b). This is likely due to the fact that brain endothelial proliferation and sprouting become very restricted after the postnatal period[1].

To test whether epileptiform activity also affects neonatal angiogenesis, we administered the cholinergic muscarinic agonist, pilocarpine for 10 days, which induced mild generalized seizures without tonic-clonic convulsions lasting for ~2 hours (Supplementary Figure 3). These seizures caused robust reductions of cortical vessel density in neonates (Figure 1h, Supplementary Figure 2a, Supplementary Figure 4), but did not affect the adult microvasculature (Figure 1h). We tested a second seizure mechanism, independent of cholinergic stimulation by intracortical injection of tetanus toxin, which blocks neurotransmission in inhibitory interneurons. This treatment also induced non-convulsive seizures, after which we observed significant vessel reductions in the cortex, contralateral (Figure 1i) and ipsilateral (data not shown) to the injection. Botulinum toxin, a structurally similar molecule that blocks excitatory neurotransmission, had no effect on vessels, supporting the conclusion that only hyperactivity affects microvascular remodeling (Figure 1i).

To determine if hyperactivity blocks vessel formation through stress or energetic depletion, we administered the glucocorticoid dexamethasone, a model of stress, or the glucose analogue, 2-deoxyglucose, to impair glucose metabolism. However, neither of these treatments affected the cortical vasculature (Figure 2a). Furthermore, hyperstimulation was not associated with cell death, changes in cell density, or microglia activation (Supplementary Figure 5). This suggests that reductions in vessel density are not secondary to homeostatic alterations, but a direct vascular response to hyperactivity.

We further examined the effect of hyperactivity on endothelial proliferation by repeated bromodeoxyuridine (BrdU) administration and found that both auditory stimulation and seizures markedly decreased proliferation selectively in endothelial cells (Figure 2b–f, Supplementary Figure 6). To determine how activity influenced vascular plasticity, we performed *in vivo* transcranial two-photon time-lapse imaging of mice expressing green fluorescent protein in their endothelium (Tie2-GFP). We found that administration of pilocarpine for 5 days caused 90% fewer microvascular formations (Figure 2g,h,j), resulting in a significant reduction in vascular length added (Figure 2k). In contrast, the number of eliminated branches was not different from controls (Figure 2g,i,j). These results demonstrate that perturbed activity does not cause vascular regression, but rather arrests the proliferation and sprouting of new vessels.

Nitric oxide (NO) is released during neural activation and is known to modulate angiogenesis[16]. We therefore asked whether NO is involved in the anti-angiogenic effects of neural activity. In the brain, NO is produced by three nitric oxide synthase (NOS) isoforms; eNOS and nNOS are constitutively active in endothelial cells and neurons respectively, and inducible NOS (iNOS), which increases during inflammation, but is also present at baseline in glia and neurons[17–19]. Studies using NO donors or NOS overexpression have shown that NO is pro-angiogenic at moderate levels and anti-angiogenic at high physiologic concentrations[20–22]. Remarkably, we found that activity-mediated vessel reductions were

completely prevented by administration of a broad NOS inhibitor (L-NAME), but not its enantiomer D-NAME (Figure 3a,b). We then exposed isoform-specific loss-of-function mutants to auditory stimulation and found that mice lacking nNOS or iNOS were completely protected against activity-mediated vessel reductions, while eNOS knockouts were not (Figure 3c,d). nNOS is expressed in subtypes of inhibitory interneurons[23], which are over-activated during prolonged stimulation and glial iNOS also responds to changes in neuronal activity[18]. Therefore it is likely that activity-dependent NO production is responsible for the vascular effects observed (Supplementary Figure 7, Supplementary discussion 2). While we found no changes in nNOS and iNOS protein levels following stimulation (Supplementary Figure 8a), these isoforms produce nitric oxide very efficiently, therefore modest changes in their catalytic activity have strong effects on NO production. The anti-angiogenic effects of hyperactivity did not appear to be mediated by vascular endothelial growth factor (VEGF) because stimulation had no measurable effect on VEGF or VEGF receptors levels (Supplementary Figure 8b–d).

Our data shows that perturbation of neural activity reduces vascular growth by 70–80% following activity paradigms and near 100% following seizures. This growth arrest is likely to impact micro-regional tissue oxygenation because the brain, unlike other organs, has high energetic demand, minimal energy storage, and no un-perfused microvascular reserve[1]. To determine the effects of vessel reductions on brain homeostasis, we devised a method to spatially correlate regional tissue oxygenation with the relative proximity to capillaries using the tissue hypoxia probe pimonidazole. At normal oxygen levels, no pimonidazole signal was observed in either control or hyperstimulated mice (Supplementary Figure 9). Interestingly, when mice were exposed to 8% O_2 for 1 hour, we observed a greater pimonidazole signal in mice with reduced microvascular density caused by hyperactivity (Figure 4a–d). Brain microregions distant from vessels experience lower oxygen tension at baseline and following neural activation[24,25]. Accordingly, in control mice, we observed a trend toward increased pimonidazole signal in areas further than 10 μm from blood vessels. In hyperstimulated mice, this difference was more pronounced, suggesting that reduced microvascular density impairs oxygen delivery to areas distant from capillaries (Supplementary Figure 10).

To explore the effect of this diminished oxygen delivery on neuronal connectivity we measured dendritic spine density of layer V pyramidal neurons after exposure to moderate hypoxia (8% O_2 for 48 hours). Mice that had previously been exposed to repetitive auditory stimuli experienced a reduction in spine density in auditory cortex, specifically in areas distant from capillaries, while unstimulated mice did not experience spine loss (Figure 4e,f). This demonstrates that the observed microvascular reductions can cause synaptic loss after a mild reduction in environmental oxygen and suggests that other metabolic challenges or increases in demand may have similar effects. In addition to changes in spine number, our results suggest that impaired oxygen delivery to intercapillary regions may be involved in the alterations in cortical tonotopic mapping and auditory discrimination observed after repetitive auditory stimulation in neonates[26–28].

We next sought to determine if microvascular reductions were long-lasting by exposing mice to auditory stimulation and assessing vessel density at various time intervals. Neonates

given a 5-day auditory stimulus completely regained normal vascular density 1 month later (Figure 4g), likely because hyper-stimulation was stopped before the end of the first postnatal month, when substantial angiogenesis is still ongoing[1]. However, when auditory stimulation was extended to at least 15 days, vessel density did not return to normal even after 5 months (Figure 4h). This indicates the existence of a critical period during which the vasculature can recover from anti-angiogenic intervention, but after which deficits become permanent. Therefore a temporary exposure to hyperactivity in neonates causes permanent alterations in microvascular architecture, leading to deficits in oxygen delivery and impaired neuronal connectivity (Supplementary Figure 11).

Our study shows that modest alterations in baseline levels of neural activity do not affect vascular patterning, suggesting that in the postnatal period brain angiogenesis follows an autonomous developmental program. Unexpectedly, this program can be disrupted by elevated levels of nitric oxide released from neurons and glia following repetitive sensory-motor stimulation or seizures. This effect is probably maladaptive, given that such repetitive activity patterns are not likely to have been prevalent through evolution. However, these findings raise the concern that early childhood seizures[29] or exposure to repetitive auditory and other sensory-motor stimuli, which are common in modern society[30], could have lifelong repercussions on the cortical microvasculature, its oxygen delivery capabilities, and the homeostasis of neural cells. In addition, it may make the brain vulnerable to conditions of reduced oxygen supply or microvascular pathology such as hypertension, diabetes and aging.

Full Methods

Mice

Wild type mice (Charles River), Tie2-GFP endothelial reporter (Jackson Labs #003658), Thy1-YFP (Jackson Labs#003782), neuronal nitric oxide synthase knockdown mice (Jackson Labs #002986), inducible NOS knockout mice (Jackson Labs #002609), and endothelial NOS knockout mice (Jackson Labs #002684) were on a C57Bl6 background. Mice between postnatal age p5 and p200 were used. In all experiments littermates were assigned to treatment or control groups and equally distributed by sex and body weight (though neither of these factors influence vessel density, Supplementary Figure 12d,e). Pups were housed jointly with their mother except for the duration of stimulation or injections. For adult experiments 9-week old females were used. Sample sizes for each experiment were chosen based on the size of the litter (typically N=5 per group) and in some cases repeated to confirm with different litters. Experimental protocols were in accordance with the relevant guidelines and regulations of the Institutional Animal Care and Use Committee at Northwestern University and Yale University.

Treadmill exercise, auditory and whisker stimulations

In our exercise experiments, pups starting at age p15 were placed in individual lanes on a custom-made treadmill to induce moderate running speeds (15 cm/s) over 45 min, 3 times daily for 5 days.

For auditory experiments, pups were separated from their mothers and exposed overnight to 10 hours of a variety of sounds (40–75dB) consisting of white and pink noise, tones over a range of frequencies, frequency sweeps, recordings of rodent vocalizations, and other natural sounds. Littermate controls were also separated from their mothers and kept in a quiet room. Stimulation began as early as p15 and lasted 5, 10, or 15 days. For long-term experiments, mice were stimulated between 15 and 30 days and then returned to their home cages for 1, 3 or 5 months before sacrifice.

To unilaterally stimulate whiskers, unilateral whisker trimming was performed daily and mice were subsequently placed into a cage with a continuous airflow for 10 hours over 8 days. Vessel density in the stimulated barrel cortex (contralateral to the stimulated whiskers) was compared to the unstimulated (trimmed) cortical region.

Pilocarpine-induced seizures

Pilocarpine was administered intraperitoneally (IP) (72 mg/kg, P6503, Sigma) as early as p5. This dosage is substantially lower than that used to induce chronic epilepsy[31]. Starting at p7 mild seizures were observed following injection. These were characterized by reduced exploratory behavior, excessive salivation, forelimb clonus, and occasional head bobbing, which ceased after 2 hours. Mice received daily injections over 10 days. No evidence of spontaneous seizures was noted during this period.

Intracortical tetanus and botulinum toxin injections

For intracortical injections, a craniotomy is made over the cingulate cortex of anesthetized mice by thinning the skull with a dental drill and using a fine needle to remove a small (100 μm diameter) piece of skull. Using a fine glass capillary mounted to a stereotaxic apparatus, tetanus toxin[32] (25ng; 190A, List Biological Labs) or botulinum toxin (0.03ng; 128A, List Biological Labs) was diluted in 7 μl of artificial cerebral spinal fluid (ACSF) and injected 500 μm into the cingulate cortex. A CamKII-Tomato adeno-associated reporter virus was added to the injection mix to demarcate the injected area for later relocation. An equivalent volume of ACSF with virus was injected into control mice. Mice experienced spontaneous seizures, demonstrated by head bobbing and facial spasms a few days after injection, which continued to occur until they were sacrificed 10 days later.

Models of impaired metabolism and stress and nitric oxide manipulations

Starting at p15 mice were given 10 daily IP injections of either 2-deoxyglucose (2-DG, 10mg/kg; D8375, Sigma), which impairs glucose metabolism, or the glucocorticoid dexamethasone (5 mg/kg, D4902, Sigma), which is a widely used model of stress[33]. To manipulate nitric oxide levels, the nitric oxide inhibitor L-NAME (50 mg/kg, N5751, Sigma), the nitric oxide substrate L-arginine[34] (50mg/kg, A5006, Sigma), and the L-NAME enantiomer D-NAME (50mg/kg, N4770, Sigma) were diluted in saline and injected IP 30 minutes prior to onset of each stimulation session.

In vivo transcranial two-photon time-lapse imaging

Cerebral blood vessels were imaged in Tie2-GFP endothelial reporter mice. Neonatal time lapse imaging was performed on the two-photon microscope as previously described[1].

Briefly, mice were anesthetized with isoflurane and the skull was exposed with a midline scalp incision. A 1 mm diameter skull region over the somatosensory cortex was thinned with a microsurgical blade to a final thickness of ~30 μm. The surrounding skull was attached to a custom-made steel plate to stabilize the head while imaging. A CCD camera image of skull blood vessels allowed for relocation of the imaging area. The first time point was acquired at p15, and then mice received daily IP injections of pilocarpine or saline for 5 days. One day after the final injection, mice were prepared for imaging and blood vessels were re-located and imaged for a second time point.

Hypoxia stress test

Mice were exposed to 15 days of auditory stimulus or 10 days of pilocarpine-seizures. Mice were then injected IP with Hypoxyprobe-1 (pimonidazole HCL 50mg/kg; HP1-1000Kit, Hypoxyprobe Inc.) to label hypoxic tissue. Note that the threshold for pimonidazole detection is <10 mmHg tissue O_2 and may therefore not detect mild O_2 reductions. 10 minutes after injection of the probe, mice were placed into a hypoxic chamber set at 8% oxygen for 1 hour. Mice were anesthetized, while still in the hypoxic chamber and, when they were no longer responsive, they were removed and immediately sacrificed by transcardial perfusion.

Imaging of dendritic spines in hypoxic brains

Dendritic spines were visualized in Thy1-YFP H line reporter mice, which express yellow fluorescent protein in layer V pyramidal projection neurons. Mice were given 10 days of auditory stimulation and then placed in a hypoxic chamber at 8% for 48 hours. Control littermates received no stimulation but were exposed to hypoxia. Animals were injected IV with NHS biotin to label vessels and sacrificed by transcardial perfusion. In a separate group of mice, animals were exposed to auditory stimulation or control conditions and immediately sacrificed to determine baseline changes in spine density.

Tissue collection and histology

Mice were anesthetized by IP injection with ketamine/xylazine (120 mg ml^{-1}/10 mg ml^{-1}) and sacrificed by transcardial perfusion using 4% paraformaldehyde (PFA). Brains were postfixed, bathed in sucrose and cut on the cryostat into 50 μm coronal sections. For western blotting, fresh cortices were dissected from the rest of the brain under a dissecting microscope and flash frozen. For brain weight measurements, unperfused brains were extracted and immediately weighed.

Vessels were stained in fixed tissue using collagen IV antibody (1:250; -ab19808, Abcam), Glut-1 (1:100; 2186307, Millipore) or isolectin B4 (1:50; B1205, Vector Labs) as previously described[1]. Additional vessel labeling was achieved by transcardial injection of fluorescein-tomato-lectin (200 μl; FL1171, Vector Labs) or NHS-biotin (300 mg/kg; 2027, Thermo), which required a conjugated streptavidin counterstain.

For BrdU labeling, mice were injected IP every second day with BrdU (5 mg/kg; B5002, Sigma). Brain sections were washed, denatured with 5M HCl for 15 minutesand incubated with rat anti-BrdU (1:400, OBT0030, AbDSerotec).

Staining for other cell types was performed using the following antibodies: NeuN (1:250; MAB377, Millipore) to label neurons, IBA1 (1:200; 019-19741, Wako) for microglia, pdgf receptor beta (1:100; AF1042, R&D) for pericytes, VEGF (1:100; ab46154, Abcam). To label VEGF pathway components VEGFR2 (1:1000; 55B11 Cell Signaling), Phospho-VEGFR2 (Tyr 1175) (1:1000; 19A10, Cell Signaling), Phospho-VEGFR2 (Tyr951) (1:1000; 7H11, Cell Signaling), and VEGFR1 (1:1000; ab32152, Abcam) were used. Hypoxyprobe-1 (1:50, HP1-1000Kit, Hypoxyprobe Inc.) was used to detect injected pimonidazole, and C-fos (1:100; F7799, Sigma) was used to detect immediate early protein detection. DAPI (1:1000; 9542, Sigma) was used to quantify cellular densities.

A TUNEL detection kit (11684817910, Roche) and cleaved Caspase-3 antibody (1:100, Millipore; 559565, BD Pharmingen) were used to label dying and apoptotic cells. DNAse treatment served as a positive control for TUNEL staining and a stroke induced by microembolism with 50 μm beads injected into the carotid artery was a positive control for both TUNEL and Caspase-3 labeling. AlexaFluor antibodies 488 and 555 (Life Sciences) were used throughout. For all experiments, sections from both groups were stained simultaneously, using the same batch of antibodies.

VEGF protein levels were measured with mouse VEGF Quantikine Elisa Kit (MMV00, R&D) according to the manufacturer's instructions using tissue from mice treated with pilocarpine or saline between p15-25 and assayed in triplicate.

Area selection and image acquisition for vascular quantification

Vascular density varies greatly by brain region, therefore the Paxinos and Allen brain atlas were used to carefully identify and locate cortical areas. For each area analyzed, a standard coronal section, containing the relevant cortical region, was found. Three consecutive sections were selected from each mouse brain region and standardized regions were located bilaterally using the atlas (6 regions of interest were obtained for quantification in each brain, see Supplementary Figure 12a). To ensure uniformity of the sections, special care was taken that the angle of cryo-cutting was standard for all brains and cutting was performed during a single session.

Primary auditory cortex, sensory barrel cortex, and primary motor cortex were quantified for auditory, whisker, and motor experiments respectively. Control areas were always chosen from the same section: cingulate cortex used as a control for auditory and whisker experiments and the piriform cortex used for motor stimulation. For pilocarpine seizures, 2DG-, and dexamethasone-treated brains, the cingulate cortex was quantified.

Using a Leica 0.8 NA 20x lens, an image of the entire cortical region of interest was obtained on a confocal microscope (Leica SP5) at 1x zoom, 1 μm step size, 1024×1024 resolution, and a scan speed of 600Hz. Imaging for an individual experiment was performed in one session, with uniform laser intensity and gain parameters used between control and experimental groups.

Vessel density quantification and laminar layer determination

For quantification, vessels were labeled with isolectinB4, NHS-biotin, or collagen IV. Z-projections were made from a fixed number of optical sections. All quantifications were done in a blinded manner. Vascular length was quantified automatically using a custom-made ImageJ (NIH) macro in which vessels were thresholded to create a binary mask, despeckled, and skeletonized. Skeletonized vessels were used to obtain vessel length in microns (Supplementary Figure 12a). Blinded manual counts of blood vessel branches were performed using Image J Cell Counting software (Supplementary Figure 12b). To ensure accurate counts, 6 cortical regions and more than 2000 branches were counted in each animal. To quantify individual laminar layers, we used previously published measurements of cortical layers in barrel, auditory, and motor cortices[35–37] to divide our images into the relevant laminae.

Other cellular quantifications

We have previously shown that endothelial BrdU can be accurately separated from non-endothelial BrdU as well as peri-vascular BrdU using confocal images[1]. For BrdU, high-resolution confocal images were obtained using a Leica 1.3 40x HCLX PL APO oil immersion lens in the cingulate cortex for pilocarpine-treated mice, and in the auditory and cingulate cortex for auditory-stimulated mice. Z-projections of a standardized thickness were made and BrdU positive endothelial and non-endothelial cells were counted on ImageJ Cell Counting software.

Quantification of total cell number (DAPI), neuron, and microglia number was performed in the cingulate cortex using ImageJ Cell Counting software. All manual counting was done in a blinded fashion.

For co-localization of neurons with c-Fos, neurons and c-Fos images were separated and quantified individually on ImageJ Cell counter so that the percentage of c-fos positive neurons could be calculated.

Quantification of microvasculature in vivo

In vivo two-photon image stacks were cut to a standard thickness of 150 μm and vessels were quantified in a blinded manner. To measure total vessel length, we used Fiji Simple Neurite Tracer, which allowed us to trace individual vessels in 3 dimensions. Total vessel length was determined for first and final time points and percent difference was calculated.

ImageJ was used to quantify elimination and formation of branches *in vivo* by comparing first and second time points. New branches consisted of new sprouts (counted as 1 new branch), sprouts which had anastomosed to form a connected vessel (counted as 1 new branch), and vessels which became fully connected at the second time point (counted as 2 new branches). Eliminated branches consisted of fully formed vessels that had retracted such that only a sprout remained (counted as 1 eliminated branch), fully formed vessels which retracted completely (counted as 2 eliminated branches), and sprouts which retracted completely (counted as 1 eliminated branch). Change in branches was determined by counting all branch points at time point 1 and then counting branches that had been added or

lost at time point 2. Percent change in branch formation and elimination were calculated by dividing the number of new or lost branches by the total number of branches at time point 1. The observed vessel changes were evenly distributed across the entire tissue volume

Statistics

For each mouse, vessel and cell density quantifications were obtained from both hemispheres of 3 coronal sections (6 images in total) and were averaged to obtain a single value.

While there is strong inter-litter consistency in vessel density, there are small but significant differences in density between litters. Therefore all of our comparisons are done within litters (both controls and experimental animals belong to a single litter). However, as most experiments utilize multiple litters, we use a normalization method to add together different litters. In each litter, the experimental group is normalized so that the control group averages to 100%, and following this normalization, multiple litters can be combined. Density values are distributed normally and a one tailed student's t-test assuming equal variance was used to compare groups. Spine density and hypoxia was compared between areas near and far from vessels, the stimulated and unstimulated hemispheres were compared in whisker-stimulated mice, and all other comparisons were performed between control and experimental groups.

Tissue hypoxia quantification

Sections were co-stained with collagen IV and pimonidazole antibodies and images were obtained on Leica HyD detectors, confocal photon-counting mode using a 1.0 NA 20x lens at 1x zoom, 1 μm step size, 1024×1024 resolution, and a scan speed of 600Hz. Primary auditory cortex was imaged following auditory treatment and cingulate cortex was used for pilocarpine seizure treatments and images were projected to uniform thickness (5 μm).

We designed an ImageJ macro to quantify pimonidazole staining. In this, blood vessels are thresholded and a mask is created and projected over the pimonidazole staining so that only pimonidazole signal in non-vascular areas is quantified. A histogram of the pimonidazole staining is obtained which shows the distribution of the brightness of individual pixels. We use 8-bit images, therefore brightness is distributed over 256 bins, 0 representing no detectable signal and 256 representing the brightest. Because the non-vascular area may vary, brightness values were converted to percentages of the total number of pixels counted. Values for each brightness bin (0–256) are averaged across 6 images for each mouse, to obtain a single average histogram per animal. Group averages for each brightness bin are obtained by averaging the brightness values of individual animals and one-tailed t-tests are performed in each brightness bin to compare mice in different experimental groups.

To determine the differences in pimonidazole brightness near and far from capillaries, a histogram representing tissue closer than 10 μm to vessels was compared to areas more than 10 μm away from the nearest vessel. This was done automatically using a custom-made ImageJ macro. In this macro a vessel mask was created and a histogram of total pimonidazole staining was obtained. Then the vessel mask was dilated to 10 μm to obtain a

second histogram in the area further from vessels. This second histogram was subtracted from the initial histogram to obtain a value for the area closer than 10 μm to vessels.

Dendritic spine density quantification

NHS biotin-injected brains were counterstained with fluorescently-labeled streptdavidin to label vessels and sections were imaged on the confocal microscope using a Leica 1.4 NA 63x lens at 4x zoom at 1 μm step size. 16 images (1024 × 1024 pixel each) were acquired to cover layers 2/3 and 4 of the auditory cortex and stitched together to reconstruct the dendritic projections. Tiled stacks were z-projected to a standardized thickness (5 μm) for quantification and 4 to 6 images were quantified for each animal. Using a custom-made ImageJ macro, vessels were thresholded and a mask was created. The vessel mask was dilated to 20 μm, to create a selection which outlined the area 20 μm from the nearest vessel. This selection was projected over the image of the dendrites to create a border between areas “near” and “far”.

Images were quantified blinded to treatment. In each image we excluded dendrites that were out of focus or displayed weak YFP labeling, such that individual spines could not be identified. The remaining dendrites were traced to determine their total length in areas “near” or “far” from vessels. Spines were counted manually using ImageJ Cell Counter and density “near” and “far” from vessels was determined by dividing by the length of the dendrites quantified. An average density “near” and “far” was determined for each animal and group averages “near” and “far” were compared using a student’s t-test.

Supplementary Material

Refer to Web version on PubMed Central for supplementary material.

Acknowledgments

The authors appreciate the expert advice of W. Sessa, M. Simons, and F. Moraes. A. Schain helped with design of ImageJ macros and GP. Flowers critically read the manuscript. This study was supported by the following Grants: R01AG027855 and R01HL106815 (JG); F31NS068041 (CW) and AHA# 10POST2570007 (CF).

References

1. Harb R, Whiteus C, Freitas C, Grutzendler J. In vivo imaging of cerebral microvascular plasticity from birth to death. Journal of cerebral blood flow and metabolism : official journal of the International Society of Cerebral Blood Flow and Metabolism. 2013; 33:146–156. [PubMed: 23093067]
2. Spitzer NC. Electrical activity in early neuronal development. Nature. 2006; 444:707–12. [PubMed: 17151658]
3. Lam C, Yoo T, Hiner B, Liu Z, Grutzendler J. Embolus extravasation is an alternative mechanism for cerebral microvascular recanalization. Nature. 2010; 465:478–482. [PubMed: 20505729]
4. Carmeliet P, Tessier-Lavigne M. Common mechanisms of nerve and blood vessel wiring. Nature. 2005; 436:193–200. [PubMed: 16015319]
5. Dunning HS, Wolff HG. The relative vascularity of various parts of the central and peripheral nervous system of the cat and its relation to function. The Journal of Comparative Neurology. 1937; 67:433–450.

6. Black JE, Isaacs KR, Anderson BJ, Alcantara AA, Greenough WT. Learning causes synaptogenesis, whereas motor activity causes angiogenesis, in cerebellar cortex of adult rats. Proc Natl Acad Sci U S A. 1990; 87:5568–5572. [PubMed: 1695380]
7. Wei L, Erinjeri JP, Rovainen CM, Woolsey TA. Collateral growth and angiogenesis around cortical stroke. Stroke; a journal of cerebral circulation. 2001; 32:2179–84.
8. Whitaker VR, Cui L, Miller S, Yu SP, Wei L. Whisker stimulation enhances angiogenesis in the barrel cortex following focal ischemia in mice. Journal of cerebral blood flow and metabolism : official journal of the International Society of Cerebral Blood Flow and Metabolism. 2007; 27:57–68. [PubMed: 16670699]
9. Rao S, et al. A direct and melanopsin-dependent fetal light response regulates mouse eye development. Nature. 201310.1038/nature11823
10. Vasudevan A, Long JE, Crandall JE, Rubenstein JL, Bhide PG. Compartment-specific transcription factors orchestrate angiogenesis gradients in the embryonic brain. Nat Neurosci. 2008; 11:429–439. [PubMed: 18344991]
11. Margolis DJ, et al. Reorganization of cortical population activity imaged throughout long-term sensory deprivation. Nature neuroscience. 2012; 15:1539–46. [PubMed: 23086335]
12. Zuo Y, Yang G, Kwon E, Gan WB. Long-term sensory deprivation prevents dendritic spine loss in primary somatosensory cortex. Nature. 2005; 436:261–5. [PubMed: 16015331]
13. Crochet S, Petersen CCH. Correlating whisker behavior with membrane potential in barrel cortex of awake mice. Nature neuroscience. 2006; 9:608–10. [PubMed: 16617340]
14. Beloozerova IN, Sirota MG, Swadlow HA. Activity of Different Classes of Neurons of the Motor Cortex during Locomotion. J Neurosci. 2003; 23:1087–1097. [PubMed: 12574439]
15. Licht T, Keshet E. Delineating multiple functions of VEGF-A in the adult brain. Cellular and molecular life sciences : CMLS. 2013; 70:1727–37. [PubMed: 23475068]
16. Rudic RD, et al. Direct evidence for the importance of endothelium-derived nitric oxide in vascular remodeling. The Journal of clinical investigation. 1998; 101:731–6. [PubMed: 9466966]
17. Keilhoff G, et al. Patterns of nitric oxide synthase at the messenger RNA and protein levels during early rat brain development. Neuroscience. 1996; 75:1193–1201. [PubMed: 8938752]
18. Buskila Y, Amitai Y. Astrocytic iNOS-dependent enhancement of synaptic release in mouse neocortex. Journal of neurophysiology. 2010; 103:1322–8. [PubMed: 20071630]
19. Van den Tweel ERW, et al. Expression of nitric oxide synthase isoforms and nitrotyrosine formation after hypoxia-ischemia in the neonatal rat brain. Journal of neuroimmunology. 2005; 167:64–71. [PubMed: 16112751]
20. Ridnour, La, et al. Nitric oxide regulates angiogenesis through a functional switch involving thrombospondin-1. Proceedings of the National Academy of Sciences of the United States of America. 2005; 102:13147–52. [PubMed: 16141331]
21. Heller R, Polack T, Gräbner R, Till U. Nitric oxide inhibits proliferation of human endothelial cells via a mechanism independent of cGMP. Atherosclerosis. 1999; 144:49–57. [PubMed: 10381277]
22. Jones MK, Tsugawa K, Tarnawski AS, Baatar D. Dual actions of nitric oxide on angiogenesis: possible roles of PKC, ERK, and AP-1. Biochemical and Biophysical Research Communications. 2004; 318:520–528. [PubMed: 15120632]
23. Perrenoud Q, et al. Characterization of Type I and Type II nNOS-Expressing Interneurons in the Barrel Cortex of Mouse. Frontiers in neural circuits. 2012; 6:36. [PubMed: 22754499]
24. Kasischke KA, et al. Two-photon NADH imaging exposes boundaries of oxygen diffusion in cortical vascular supply regions. Journal of cerebral blood flow and metabolism : official journal of the International Society of Cerebral Blood Flow and Metabolism. 2011; 31:68–81. [PubMed: 20859293]
25. Devor A, et al. “Overshoot” of O_2 is required to maintain baseline tissue oxygenation at locations distal to blood vessels. The Journal of neuroscience : the official journal of the Society for Neuroscience. 2011; 31:13676–81. [PubMed: 21940458]
26. Chang EF, Merzenich MM. Environmental noise retards auditory cortical development. Science (New York, NY). 2003; 300:498–502.
27. Zhang LI, Bao S, Merzenich MM. Persistent and specific influences of early acoustic environments on primary auditory cortex. Nature neuroscience. 2001; 4:1123–30. [PubMed: 11687817]

28. Strata F, et al. Perinatal anoxia degrades auditory system function in rats. Proceedings of the National Academy of Sciences of the United States of America. 2005; 102:19156–61. [PubMed: 16365292]
29. Sillanpää M, Jalava M, Kaleva O, Shinnar S. Long-term prognosis of seizures with onset in childhood. The New England journal of medicine. 1998; 338:1715–22. [PubMed: 9624191]
30. Village EG. Noise: A Hazard for the Fetus and Newborn. Pediatrics. 1997; 100:724–727. [PubMed: 9836852]
31. Arida RM, Scorza FA, de Araujo Peres C, Cavalheiro EA. The course of untreated seizures in the pilocarpine model of epilepsy. Epilepsy Research. 1999; 34:99–107. [PubMed: 10210024]
32. Wykes RC, et al. Optogenetic and potassium channel gene therapy in a rodent model of focal neocortical epilepsy. Science translational medicine. 2012; 4:161ra152.
33. Sorrells SF, Caso JR, Munhoz CD, Sapolsky RM. The stressed CNS: when glucocorticoids aggravate inflammation. Neuron. 2009; 64:33–9. [PubMed: 19840546]
34. Palmer RM, Ashton DS, Moncada S. Vascular endothelial cells synthesize nitric oxide from L-arginine. Nature. 1988; 333:664–6. [PubMed: 3131684]
35. Lefort S, Tomm C, Floyd Sarria JC, Petersen CCH. The excitatory neuronal network of the C2 barrel column in mouse primary somatosensory cortex. Neuron. 2009; 61:301–16. [PubMed: 19186171]
36. Oviedo HV, Bureau I, Svoboda K, Zador AM. The functional asymmetry of auditory cortex is reflected in the organization of local cortical circuits. Nature neuroscience. 2010; 13:1413–20. [PubMed: 20953193]
37. Saikali S, et al. A three-dimensional digital segmented and deformable brain atlas of the domestic pig. Journal of neuroscience methods. 2010; 192:102–9. [PubMed: 20692291]
38. Risser L, Plouraboué F, Cloetens P, Fonta C. A 3D-investigation shows that angiogenesis in primate cerebral cortex mainly occurs at capillary level. International journal of developmental neuroscience : the official journal of the International Society for Developmental Neuroscience. 2009; 27:185–96. [PubMed: 19038323]
39. Alvarez-Buylla A, Lim DA. For the Long Run. Neuron. 2004; 41:683–686. [PubMed: 15003168]
40. Dawson TM, Dawson VL, Snyder SH. A novel neuronal messenger molecule in brain: the free radical, nitric oxide. Annals of neurology. 1992; 32:297–311. [PubMed: 1384420]
41. Amatore C, et al. Nitric oxide release during evoked neuronal activity in cerebellum slices: detection with platinized carbon-fiber microelectrodes. Chemphyschem : a European journal of chemical physics and physical chemistry. 2006; 7:181–7. [PubMed: 16353265]
42. Ferrero R, Rodríguez-Pascual F, Miras-Portugal MT, Torres M. Comparative effects of several nitric oxide donors on intracellular cyclic GMP levels in bovine chromaffin cells: correlation with nitric oxide production. British journal of pharmacology. 1999; 127:779–87. [PubMed: 10401570]
43. Heller R, Polack T, Gräbner R, Till U. Nitric oxide inhibits proliferation of human endothelial cells via a mechanism independent of cGMP. Atherosclerosis. 1999; 144:49–57. [PubMed: 10381277]
44. Jones MK, Tsugawa K, Tarnawski AS, Baatar D. Dual actions of nitric oxide on angiogenesis: possible roles of PKC, ERK, and AP-1. Biochemical and Biophysical Research Communications. 2004; 318:520–528. [PubMed: 15120632]
45. Ridnour, La, et al. Nitric oxide regulates angiogenesis through a functional switch involving thrombospondin-1. Proceedings of the National Academy of Sciences of the United States of America. 2005; 102:13147–52. [PubMed: 16141331]
46. Amitai Y. Physiologic role for “inducible” nitric oxide synthase: a new form of astrocytic-neuronal interface. Glia. 2010; 58:1775–81. [PubMed: 20737473]
47. Uttenthal LO, et al. Neuronal and inducible nitric oxide synthase and nitrotyrosine immunoreactivities in the cerebral cortex of the aging rat. Microscopy research and technique. 1998; 43:75–88. [PubMed: 9829462]
48. Crain JM, Nikodemova M, Watters JJ. Microglia express distinct M1 and M2 phenotypic markers in the postnatal and adult central nervous system in male and female mice. Journal of neuroscience research. 201310.1002/jnr.23242

49. Van den Tweel ERW, et al. Expression of nitric oxide synthase isoforms and nitrotyrosine formation after hypoxia-ischemia in the neonatal rat brain. Journal of neuroimmunology. 2005; 167:64–71. [PubMed: 16112751]

50. Bredt DS, Snyder SH. Isolation of nitric oxide synthetase, a calmodulin-requiring enzyme. Proceedings of the National Academy of Sciences of the United States of America. 1990; 87:682–5. [PubMed: 1689048]

51. Stuehr DJ, Santolini J, Wang ZQ, Wei CC, Adak S. Update on mechanism and catalytic regulation in the NO synthases. The Journal of biological chemistry. 2004; 279:36167–70. [PubMed: 15133020]

52. Downen M, et al. Neuronal nitric oxide synthase expression in developing and adult human CNS. Journal of neuropathology and experimental neurology. 1999; 58:12–21. [PubMed: 10068309]

53. Sunkin SM, et al. Allen Brain Atlas: an integrated spatio-temporal portal for exploring the central nervous system. Nucleic acids research. 2013; 41:D996–D1008. [PubMed: 23193282]

54. Galea E, Reis D, Xu H, Feinstein D. Transient expression of calcium-independent nitric oxide synthase in blood vessels during brain development. FASEB J. 1995; 9:1632–1637. [PubMed: 8529843]

55. Crain JM, Nikodemova M, Watters JJ. Microglia express distinct M1 and M2 phenotypic markers in the postnatal and adult central nervous system in male and female mice. Journal of neuroscience research. 201310.1002/jnr.23242

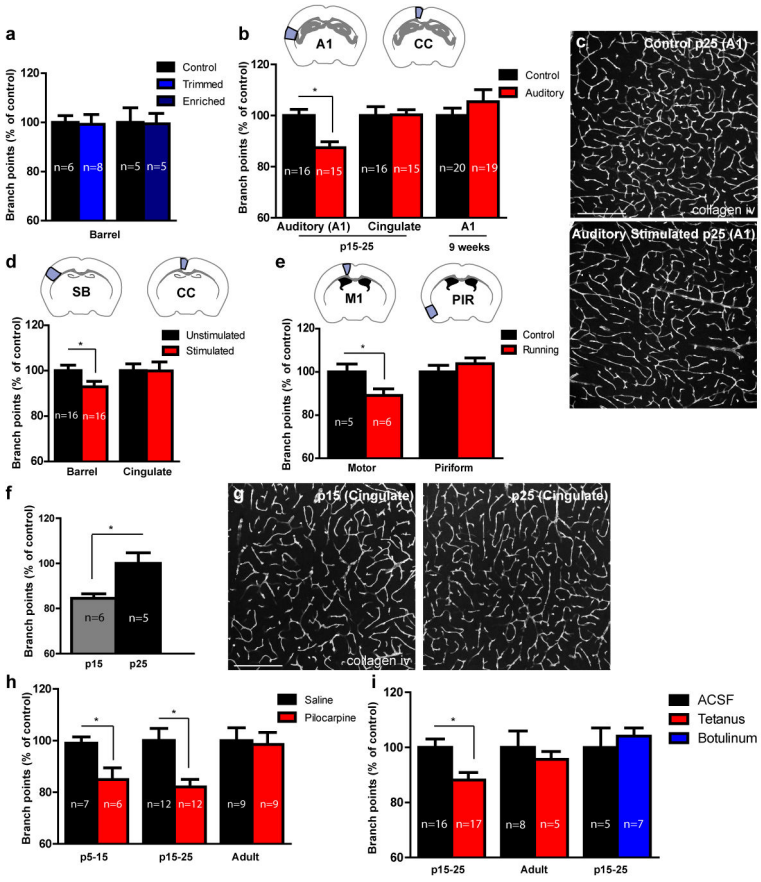

Figure 1. Elevated levels of neural activity during postnatal development lead to reduced microvascular density

(a) Cortical microvascular density is not affected by reduced neural activity caused by whisker trimming or moderate enhancement of activity by environmental enrichment. **(b–e)** Prolonged and repetitive activity through **(b,c)** auditory stimulation using a variety of tones and sounds, **(d)** increased unilateral deflection of whiskers by continuous air flow (stimulated hemisphere compared to unstimulated hemisphere contralateral to whisker-trimmed side), and **(e)** running on a treadmill, cause reduced vessel branching in auditory (A1), sensory barrel (SB), and motor (M1) cortices respectively. Vessel density in control cortical areas (cingulate-CC and piriform-PIR) was unaffected. **(b)** Auditory stimulation did not affect adult vasculature. **(f,g)** Baseline cortical angiogenesis is robust between p15-25. **(h,i)** Seizures caused by **(h)** pilocarpine or **(i)** tetanus toxin intracortical injections arrested vessel growth in neonates but not adults. **(i)** Intracortical botulinum toxin injections caused no vessel changes. Scale bars: **(c,g)** 200μm. P values one-tailed student's t-test: **(b)** p15-25:p=0.0003 (3 replicates), adult:0.16 (2 replicates), **(d)** p=0.02 (3 replicates), **(e)** p=0.02, **(f)** p=0.005, **(h)** p5–15:p=0.009, p15–25:0.002 (2 replicates), **(i)** p=0.003 (3 replicates). Bars represent SEM. N per group indicated on the bar graph.

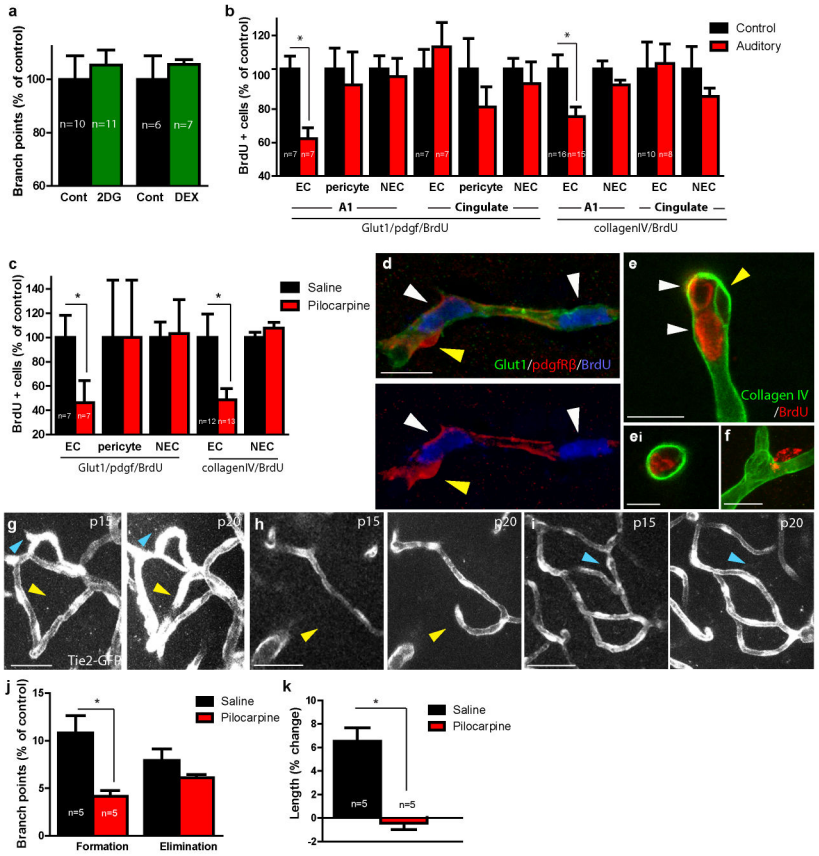

Figure 2. Neural hyperactivity reduces endothelial proliferation and new vessel formations in the neonatal cortex

(a) Daily treatment with 2-deoxyglucose (2DG) or dexamethasone (DEX) does not affect vessel density. **(b)** Auditory stimulation reduces endothelial cell (EC) proliferation, measured by BrdU, in primary auditory but not in cingulate cortex control area. Non-endothelial cell (NEC) proliferation is not affected by auditory treatment in either location (See Supplementary Figure 6). **(c)** Pilocarpine injection cause decreased endothelial cell (EC) proliferation compared to saline-injected controls. Non-endothelial (NEC) proliferation is not affected. **(d)** Representative confocal image of cortical section stained with Glut-1 (endothelium, green), pdgf receptor beta (pericytes, red), and BrdU (nuclei, blue) shows dividing endothelial cells (white arrowheads) near a nonproliferating pericyte (yellow arrowhead). **(e)** CollagenIV (green) and BrdU (red) double staining shows two proliferating EC nuclei (white arrowheads; surrounded on one side by basal lamina) and a non-proliferating pericyte (surrounded luminally and abluminally by basal lamina; yellow arrowhead). **(ei)** shows orthogonal views of an endothelial cell within the collagen IV basal lamina. **(f)** Image of a proliferating pericyte (note that proliferating pericytes are not surrounded on all sides by detectable basal lamina). **(g–k)** *In vivo* two-photon imaging reveals that hyperactivity inhibits new vessel formations. **(g–i)** Representative two-photon time-lapse images show eliminations (blue arrowheads) of a **(g)** sprout and **(i)** a vessel and formations (yellow arrowheads) of **(h)** a sprout and **(g)** a vessel between time point 1 (left panel, p15) and 2 (right panel, p20). **(j)** Percentage of vascular branches formed or

eliminated during a 5-day treatment with either pilocarpine or saline. **(k)** Significantly less vessel length increase in pilocarpine-injected mice between p15-20 than in saline-injected controls. Scale bars: **(d,e,f)** 10μm; **(ei)** 5μm, **(g–i)** 50μm. P values one-tailed student's t-test: **(b)** Glut-1/BrdU A1:p=0.001; colIV/BrdU A1:p=0.01 (2 replicates), **(c)** Glut-1/BrdU: p=0.029; colIV/BrdU:p=0.01(2 replicates), **(j)** p=0.0003, **(k)** p=0.0007. Bars represent SEM. N per group indicated on the bar graph.

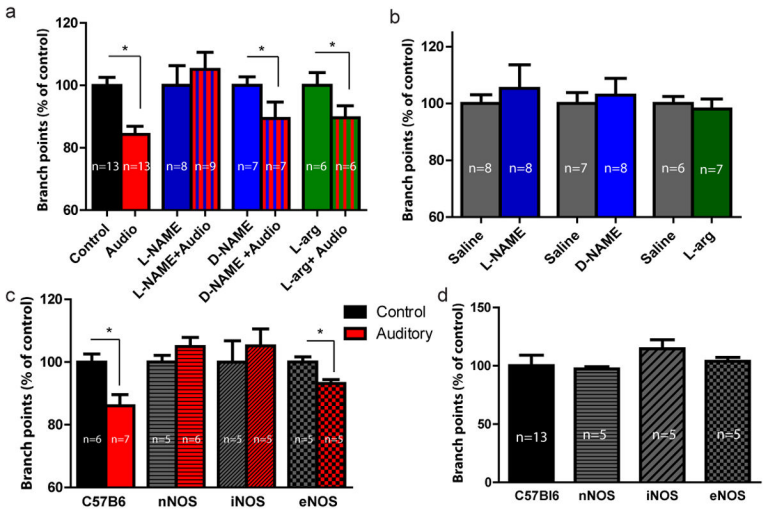

Figure 3. Inhibition of neuronal and inducible nitric oxide prevents vascular growth arrest in response to activity

(a) Mice treated with a NO inhibitor (L-NAME) prior to daily audio stimulation sessions do not experience vessel reductions following auditory stimulation between p15-25; however, pre-treatments with D-NAME and L-arginine do not rescue vessel growth-arrest. **(b)** Treatment with L-NAME, D-NAME and L-arginine in the absence of stimulation does not affect cortical vascular density. **(c)** Mice deficient in neuronal nitric oxide synthase (nNOS) or inducible NOS (iNOS) do not experience vessel growth arrest following auditory stimulation. Endothelial NOS (eNOS) deficient mice, however, do experience growth arrest. **(d)** Baseline vessel density of all three NOS deficient strains is not altered compared to wild type. P values one-tailed student's t-test: **(a)** Audio:p=0.0001 (2 replicates), DNAME:p=0.04, L-arginine:p=0.04, **(c)** C57B6:p=0.005; eNOS KO:p=0.006. Bars represent SEM. N per group indicated on the bar graph.

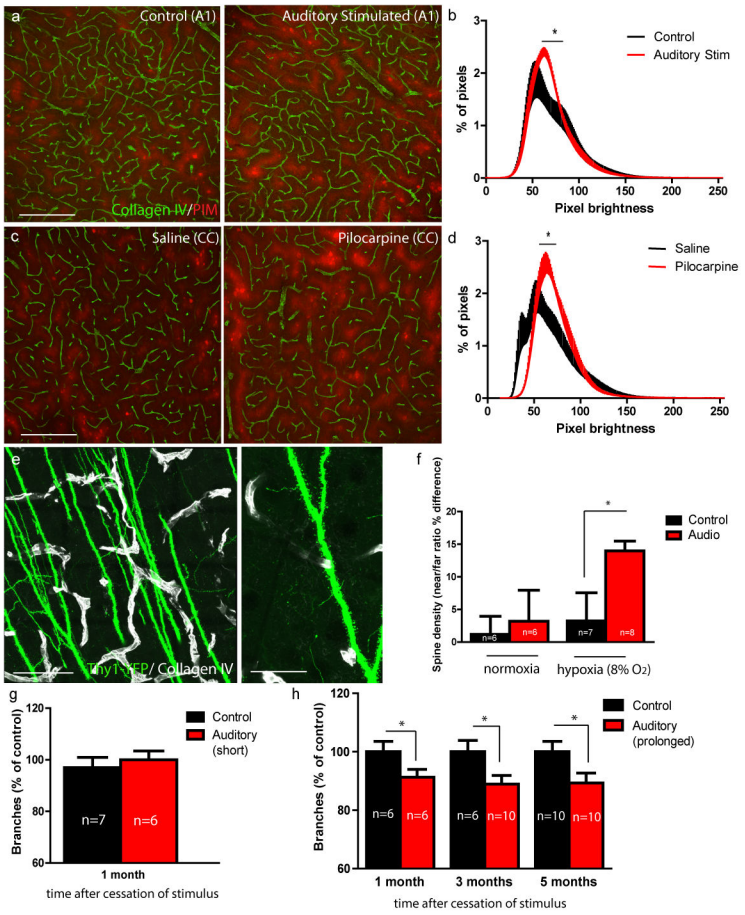

Figure 4. Activity-mediated microvascular deficits are long-lasting and affect brain oxygenation and dendritic spine stability in areas distant from capillaries

(a–d) Activity-mediated vessel reductions lead to increased levels of hypoxia both in **(a)** auditory-stimulated and **(b)** pilocarpine-injected neonatal mice. **(a)** Collagen IV vessel label (green) and pimonidazole tissue hypoxia label (red) in primary auditory cortex (A1) of control and auditory-stimulated mice. **(b)** Averaged distribution of pimonidazole pixel intensities shows brighter pixels in the stimulated group (the average % pixels at each pixel intensity were compared between animals for each treatment group using a t-test; N=5 control, N=4 auditory stimulated). **(c)** Representative images from the cingulate cortex (CC) of saline and pilocarpine-injected mice and **(d)** distribution of pimonidazole brightness shows increased labeling in mice stimulated with pilocarpine (N=5 animals per treatment group). **(e–f)** Dendritic spine density in layer 2/3 and 4 of auditory cortex in Thy1-YFPh mice was quantified using high-resolution confocal images. Spines per unit length (μm) of dendrite were calculated in areas closer and further than 20μm from the nearest vessel. **(e)** Left panel shows image of projecting dendrites (green) and vessels (white). Right panel is a higher magnification image of dendrite studded with spines. **(f)** Control and audio-treated mice were left in normoxia or exposed to 8% oxygen for 48 hours and spine density was quantified. **(g)** Vascular deficits following a 5 day auditory stimulation are fully recovered 1 month after the stimulus ended; **(h)** however, auditory stimulation for at least 15 days leads to permanent vessel loss up to 5 months post stimulation. Scale bars: **(a,c)** 200μm, **(e)**

100μm, inset 50μm. P values one-tailed student's t-test: **(b)** pixel brightness 63–72:$p<0.05$, **(d)** brightness 50–63:$p<0.05$, **(f)** $p=0.011$ (2 replicates), **(h)** 1 month:$p=0.04$, 3 months:$p=0.02$, 5 months:$p=0.02$ (2 replicates). Bars represent SEM. N per group indicated on the bar graph.